SYMCOMP 2019
Porto, 11-12 April 2019

DESIGN FOR CRASHWORTHINESS OF AN ELECTRIC VEHICLE

Samuel A. Cardoso[1], José L. Pereira[1] and André C. Marta[2*]

1: Instituto Superior Técnico, Universidade de Lisboa
Av. Rovisco Pais 1, 1049-001 Lisboa, Portugal
e-mail: {samuel.cardoso,jose.luis.pereira}@tecnico.ulisboa.pt

2: IDMEC, Instituto Superior Técnico, Universidade de Lisboa
Av. Rovisco Pais 1, 1049-001 Lisboa, Portugal
e-mail: andre.marta@tecnico.ulisboa.pt

Keywords: Collision, crash performance, energy absorption, optimization, Pareto front, genetic algorithm

Abstract. *Modern car design concepts should guarantee not only adequate dynamic characteristics but also meet strict environmental and safety standards. Regarding the later, some organizations and governments have defined regulations to include passive and active protection systems in vehicles as an effort to further reduce the number of road casualties. This work focused on the design of passive structures that maximize the vehicle crashworthiness, thus protecting its occupants in case of collisions. The two cases most common collision cases were considered, namely frontal impact and side impact, following the Euro NCAP frontal full width and the side pole impact test protocols, respectively. An optimal design process was adopted, based on the geometric parameterization of the structure, finite-element analysis models and the use a multi-objective genetic algorithm to find the best solutions. The solutions represent a trade-off between crash performance and weight, all subjected to additional compliance constraints. For the frontal impact case, four types of vehicles were analyzed. While for the lighter case a single primary structure was developed to absorb the corresponding energy during the impact, for the heavier vehicles a secondary structure was added. For the side impact case, several beam configurations were tested, being selected a multi-thickness beam with a quadrangular misaligned cross-sectional shape. The final geometries have proven to fulfill all the requirements, while still exhibiting a good trade-off between weight increase and energy absorption during the impact. The inclusion of a secondary structure for frontal impact proved to have satisfactory effects on the overall behavior during the crash events. It was shown that this methodology led to optimized beam configurations in an efficient matter, saving valuable engineering time in the iterative process.*

1 INTRODUCTION

Car accidents represent one of the largest causes of human losses. In the last twenty years, more than 800,000 people died on the roads of the European Union but thanks to a joint effort of governments and organizations, the casualties has been steadily declining.

Statistically, front collisions are the most frequent and fatal type of crash [1], so it is very important to design passive systems, such as airbags and front bumpers, to protect the passengers in case of an accident. Another critical collision is the lateral side impact, in particular with a pole due to the concentration of forces, that cause dangerous lateral accelerations to the human body. The use of side beams embedded in the door structure is usual to address this type of collision.

The crash structures need to be sufficiently robust to absorb as much energy as possible to protect effectively the occupants, while also designed for minimum weight not to severely impact the vehicle performance. This is particularly challenging for electric vehicles, whose chassis also stores highly flammable lithium batteries, and so any material intrusion in the event of a crash can lead to an uncontrolled fire.

The energy absorption and deceleration of the structures in case of impact can be predicted before the production phase using 3D modeling software and Finite Element Analysis (FEA). Through crashworthiness principles, it is possible to fix errors in the design stage, preventing their constly propagation to the production phase.

The present work focuses in the design of front and side crash structures of a modular vehicle developed in CEiiA, as shown in Fig.1. The common platform developed, including

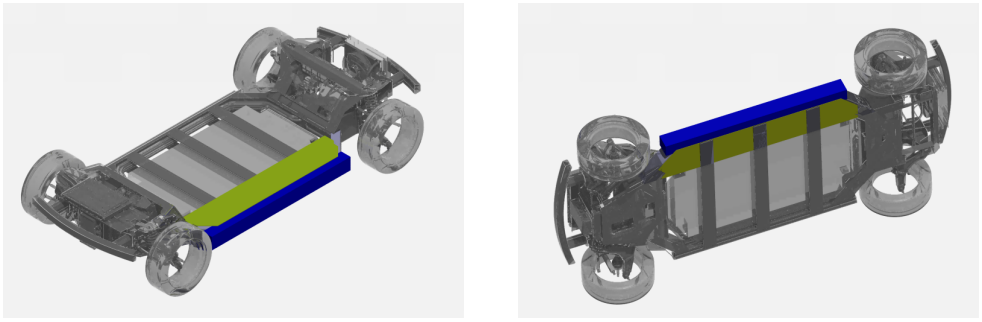

(a) top view (b) bottom view

Figure 1: Be 2.0 modular vehicle

chassis, power train, drive train and HVAC, led to the need of design effective absorptive systems for four different vehicle typologies, referred as Micro Car, Sports Car, Be 2.0 and Big Sedan, corresponding to gross weights of 1200, 1400, 1600 and 1800kg, respectively.

A procedure was developed to design the optimal structures, that fulfill the regulations of the frontal full width impact and the side-pole impact assessments from Euro NCAP, using a multi-objective optimization algorithm coupled with 3D dynamic modeling tools using Finite Element Analysis, resulting in the most efficient structures, i.e, with the highest energy absorption and lower deceleration during the impact.

2 BACKGROUND

The main theoretical elements required to tackle the proposed problem are detailed in this section, including the main regulations regarding frontal and side impacts, the crashworthiness principles, thin-walled beams, material law, heat affected zones in the soldering processes, the numerical discretization of the governing equations and the optimization algorithm used in the design procedure.

2.1 Regulations

To ensure new vehicle safety, governments and organizations have developed multiple programs around the world to regulate the minimum standards for certification. They include crash tests to analyze the damage caused to passengers using dummies equipped with accelerometers in several parts of the body.

The United Nations Economic Commission for Europe (UNECE), the European regulator, created the European New Car Assessment Programme (Euro NCAP) to independently evaluate the safety of cars.

For example, the tests described in Tab.1 are performed to evaluate the frontal collision performance. Regarding the full width frontal impact, the three criteria used to rate the

	Offset-deformable barrier	Full width rigid barrier
Velocity	64 km/h	50 km/h
Offset	40 %	-

Table 1: Euro NCAP frontal tests

vehicles about head protection in adults are the Head Injury Criteria (HIC),

$$HIC = (t_2 - t_1)\left(\frac{1}{(t_2 - t_1)}\int_{t_1}^{t_2} a\,dt\right)^{2.5}, \tag{1}$$

where $t_2 - t_1 = 15$ corresponds to the 15 milliseconds interval and a is equal to the acceleration in g, the maximum peak acceleration (a_{max}) and the mean acceleration during 3 milliseconds (a_{3ms}). The values allowed to have maximum rating score are summarized in Tab.2. These values should be taken as constraints when designing the crash structures.

Criteria	Maximum Value
HIC_{15}	700
Maximum peak acceleration	80 g
Mean acceleration during 3 msec	65 g

Table 2: NCAP head injury evaluation criteria

The side impact pole test is also extremely important since it simulates the lost of vehicle control followed by impact sideways into rigid roadside objects such as trees or

poles. For that, the vehicle is projected sideways against a rigid pole with a dummy placed in the driver's seat. Due to the localized impact, the pole intrusion in the car can be high and can cause serious injuries to the driver. The impact must occur with the pole (a circular metallic rigid structure with 354mm in diameter) with a target speed of 32km/h. The car must impact the pole in the Impact Reference Line, that results from the intersection of the vehicle's exterior surface and a vertical plane, constructed by the passage through the head's dummy center of gravity and the intersection at 75^o with the vehicle's longitudinal centerline. The evaluation criteria also includes the head injury, similarly to the frontal impact (Tab.2), but replaces the mean acceleration criterion with the condition that no direct head contact with pole can occur.

2.2 Crashworthiness Principles

The main objective of an efficient crash structure is to absorb the maximum kinetic energy without large peak accelerations.

The main parameters to evaluate crash performance are the energy absorption (EA),

$$EA = \int_0^{\delta} F(x)\, dx\,, \tag{2}$$

the average crush force (F_{av}),

$$F_{av} = \frac{EA}{\delta}\,, \tag{3}$$

the specific energy absorption (SEA),

$$SEA = \frac{EA}{M}\,, \tag{4}$$

and the crushing efficiency force (CFE),

$$CFE = \frac{F_{av}}{F_{max}}\,. \tag{5}$$

The ideal crash structure should have a CFE close to unity, meaning the initial peak force is close to the mean force during the crash event, such that the energy absorption will be maximized. In contrast, a CFE close to zero represents not only a large initial large deceleration, harmful for the vehicle passengers, but also a low energy absorption.

2.3 Thin Walled Beams

Thin walled beams have always been the preferred structures for crashworthiness for easily converting kinetic energy into plastic deformation energy, allied with reduced mass [2]. The material absorbs the maximum energy when the plastic deformation occurs in a folding mode because this type of crush leads to the total deformation of the beam.

Several works have been studied the effect of thickness, cross sectional shape, mechanical triggers and tubes filled with different types of foams.

Crashing analysis and multi-objective optimization for thin-walled structures with functionally graded thickness [3, 4, 5]. showed that variable thickness along the axial tube

direction resulted in a better absorption of energy. Cross sectional shape, including quadrangular [6], circular [7] and hexagonal [8] shapes, is by far the most relevant and studied parameter. Mechanical triggers have been proved to be a good design approach because they lead to controlled axial crushing, maximizing the energy absorption [9]. The inclusion of foams inside the beams leads to significant increments in energy absorption and a decrease in the peak force [10].

2.4 Material Law

The material formulation used is the Johnson Cook Material Law that has proven to be effective to model the material for the crash tests, where the material behavior is mostly plastic with large deformations. It models isotropic materials in elastic-plastic regimes, where a plastic behavior is only considered after the yield point. The stresses during the plastic deformation can be described by

$$\sigma = (a + b\varepsilon_n^p)\left(1 + c\ln\frac{\dot{\varepsilon}}{\dot{\varepsilon_0}}\right)\left(1 - T^{*^m}\right), \tag{6}$$

where σ is the flow stress, ε the plastic strain, a the yield Stress, b the hardening modulus, n the hardening exponent, c the strain rate coefficient, $\dot{\varepsilon}$ the strain rate, $\dot{\varepsilon_0}$ the reference strain rate and T^* the temperature exponent.

Several aluminum alloys can be modeled as strain rate insensitive [11] and, since room temperature (298 K) is assumed, temperature effects can also be neglected.

2.5 Heat Affected Zones

The Heat Affected Zones (HAZ) have special importance when parts of a structure are welded. In those joints, the material melting degrades its mechanical properties, leading to reduced yield stresses and brittleness. For several aluminum 5xxx and 6xxx series alloys, the reduction can be from 30% to 50%, so these must be taken into account [12].

2.6 Finite Elements Analysis

The finite element method (FEM) became the main analysis tool in the field of structural engineering, providing reliable results at reasonable processing time.

Since most of the crash simulation is in the plastic regime, well beyond the material yield point, with large deformations, non-linear analyses are performed. The time-marching scheme in the dynamic analyses uses an explicit formulation, for reduced computational effort, shown to be efficient in cases with many contacts and elements.

The FEM software used in the simulation of the crash structure was $Altair^{®}RADIOSS$, a leading structural analysis solver for highly non-linear problems under dynamic loads.

2.7 Multi-objective Optimization Algorithms

In the case of optimization in crashworthiness area, the goal is to maximize the SEA and the CFE simultaneously, while satisfying the design requirements. As such, a constrained multi-objective optimization algorithm is used, to solve the problem cast in the form

$$\begin{array}{lll} \text{Minimize} & f_m(\boldsymbol{x})\,, & m = 1,\ldots,M\,, \\ \text{with respect to} & \boldsymbol{x}\,, & i = 1,2,\ldots,n\,, \\ \text{subject to} & g_j(\boldsymbol{x}) \geq 0\,, & j = 1,\ldots,J\,, \\ & h_k(\boldsymbol{x}) = 0\,, & k = 1,\ldots,K\,, \\ & x_i^L \leq x_i \leq x_i^U\,, & \end{array} \tag{7}$$

where $\boldsymbol{x}$ is the set of design variables, f corresponds to the objective functions to be minimized (or maximized), g and h are the inequality and equality constraints, and x_i^L and x_i^U are the design variables upper and lower bounds.

The non-dominant optimal solutions constitute the Pareto front, representing the best compromise between the competing objectives. Among these optimal solutions, the designer can select one based on additional external trade-off criteria [13].

The Non-Sorting Genetic Algorithm (NSGA II) implemented by the function *gamultiobj* in $MATLAB^{\textcircled{R}}$ was selected to handle the multi-objective optimization problem, to easily handle the mix of discrete and continuous design variables.

3 IMPLEMENTATION

The considerations regarding material selection, geometric parametrization, FEM setup and mesh convergence, heat affected zone inclusion and optimization procedure are briefly described next.

3.1 Material Selection

The material selection for a crash structure takes into account its capability to absorb energy, durability and ease of fabrication. Thus, it was concluded that the best choice to achieve these goals is aluminum. Besides being corrosion resistant, aluminum extrusions allow to produce almost any cross section [14]. Among the most common used alloys in automotive industry, the 6xxx alloys are more easily extruded than 7xxx. The main characteristics such as Yield Strength (YS), Ultimate Tensile Strength (UTS) and Elongation at break (A) are given in Tab.3, as well as the corresponding values for HAZ.

The 6060 T64 and 6061 T4 alloys have a lower yield strength but a higher ductility, while the 6161 T6 and 6082 T6 alloys have the inverse characteristics. These choices were made to provide a wide range of Pareto optimal solutions.

3.2 Geometric Parametrization

The geometry of the structures were parametrized, for an easy change during analysis and optimization, as illustrated in Fig.2 for the front structure. The parameters include

Material	YS (MPa)	UTS (MPa)	A %	YS - HAZ (MPa)	UTS - HAZ (MPa)
6060 T64	120	180	12	60	100
6061 T4	110	180	15	95	150
6061 T6	240	260	8	115	175
6082 T6	250	290	8	125	185

Table 3: Selected aluminum alloys

thickness t, total length tl, total width tw, bumper height bh, crash box side length lc, bumper radius rb, bumper width lb, distance between crash boxes dcb and distance between structures d.

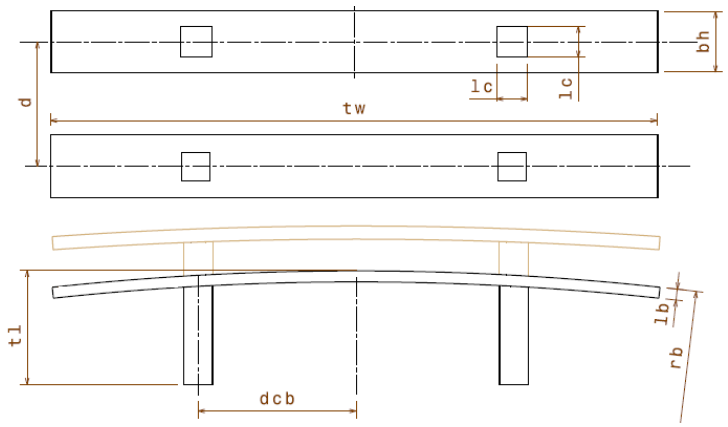

Figure 2: Parametrized geometry for both front structures

3.3 Setup of Altair® HyperMesh

Altair® *HyperMesh* was used to create the mesh, thicknesses, boundary conditions and FEM solver specific inputs. It was automatically controlled with a *Tcl* macro that included all instructions and definitions that set the specific inputs to the solver.

To evaluate the effects of different time steps and mesh sizes, a grid convergence study was performed, yielding an 8mm grid size mesh as the best compromise regarding simulation time, force–displacement curve and deformation patterns accuracy.

3.4 HAZ Evaluation

The weld zones were evaluated regarding heat effects on the overall performance of the structure. Using FEM, the elements in the junction between the crash box and the bumper were selected to define the HAZ properties. Figure 3 shows the evaluated structure and the selected elements.

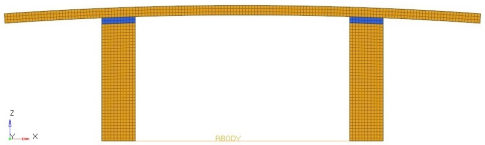

Figure 3: Bumper with the Heat Affected Zone (blue) and unchanged properties (yellow)

The crash test used was a frontal collision against a rigid wall with an imposed mass of 600kg and initial velocity of 13.8m/s. The thickness was set as constant, 6061 T6 aluminum selected and the geometry was defined with t=3.5mm, lc=90mm, tl=250mm, tw=1250mm, rb=9000mm and dcb=650mm. The resulting force–displacement curves for both non-HAZ and HAZ structures curves are presented in Fig.4.

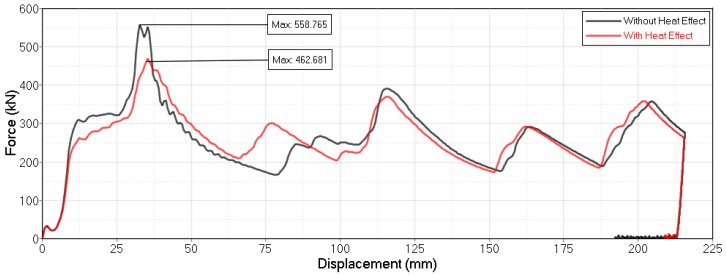

Figure 4: Effect of HAZ in force–displacement curve

A reduction of the maximum peak force in the structure with the HAZ modeled is clear, mainly due to the yield stress reduction, causing the structure to deform in this zone with a lower applied force. Thus, the HAZ revealed a significant impact in the results, making its inclusion necessary in the subsequent simulations.

3.5 Optimization Procedure

The optimization process for both structures includes several steps, from the creation of geometry to the analysis of final results by the developed script. The flowchart of the $MATLAB^{®}$ script that controls all operations is illustrated in Fig.5.

To execute the different software, the *dos* function from $MATLAB^{®}$ was used to pass the arguments to the windows command line to run the applications.

In Step 1, a $CATIA^{TM}$ macro is run with updated geometric parameters and the geometry exported. Then in Step 2, $HyperMesh^{®}$ is executed and the resulting mesh exported to $RADIOSS^{®}$, that then computes and exports the solution. In Step 3, the post-processing is done by $HyperGraph^{®}$, outputting the results in comma-separated-value format that are then analyzed by the $MATLAB^{®}$ script. Finally in Step 4, the *gamultiobj* algorithm evaluates the objective functions and constraints from each simulation. The cycle is repeated until convergence, yielding the optimal Pareto front.

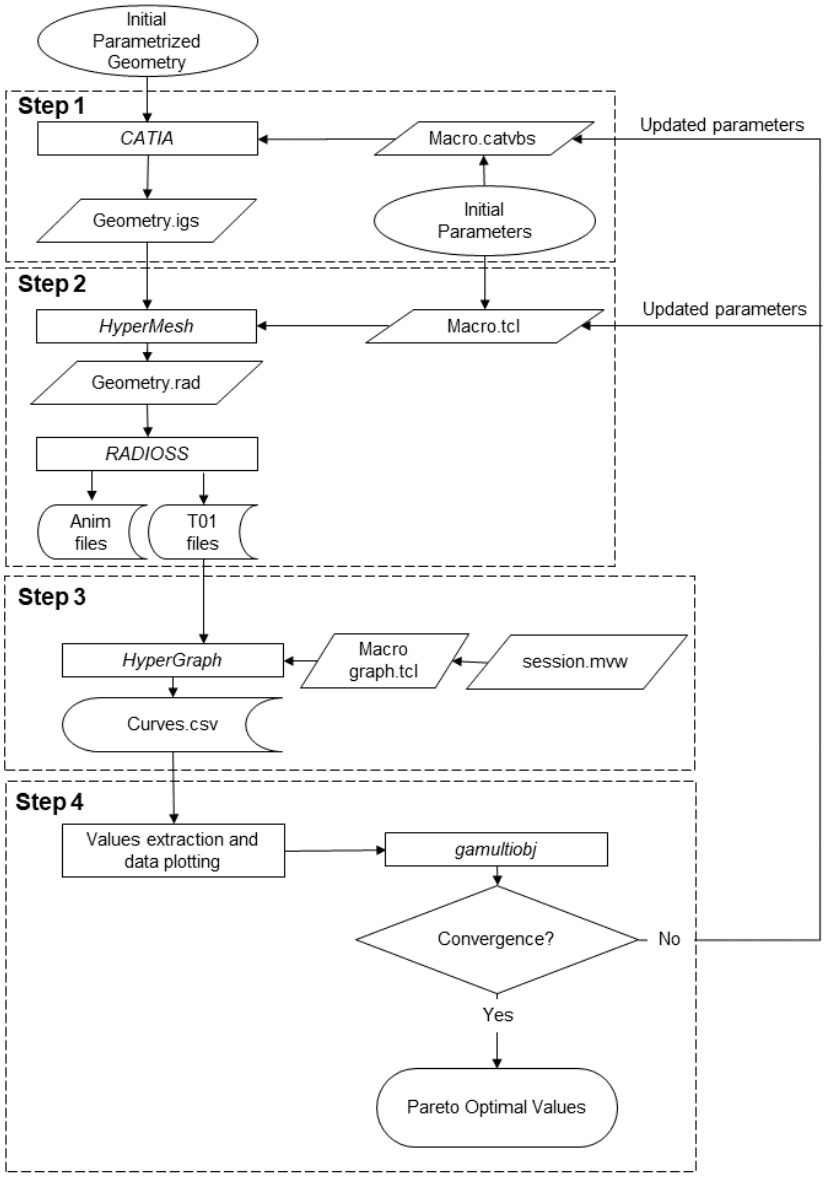

Figure 5: $MATLAB^{®}$ script flowchart

4 OPTIMAL DESIGN OF FRONT STRUCTURE

The optimizations were made always with the purpose to comply with the Euro NCAP regulations, which dictated an initial velocity of 13.8m/s in frontal impact simulations.

It was assumed that 50% of the total kinetic energy had to be absorbed by the front structures [15]. Four different vehicle were considered, each with a gross weight of 1200kg (Micro Car), 1400kg (Sports Car), 1600kg (Be 2.0) and 1800kg (Big Sedan), therefore, half their corresponding weight was imposed in the simulations. The halved weight and the initial velocity thus defined the kinetic energy to be absorbed by the structure.

For the primary front structure, corresponding to the geometry to be implemented in the Micro Car, only the values of t, tl and lc were considered for optimization. The fixed values for the other parameters are summarized in Tab.4.

Parameter	rb	lb	bh	dcb	tw
Size (mm)	9000	25	100	650	1250

Table 4: Fixed parameters for primary front structure

To optimize the secondary front structures, the values of t, lc tl rb bh and lb were considered design variables. The fixed values of dcb and tw were the same as the primary structure. The value of d was set as 400mm.

Only simple shapes were chosen to minimize manufacturing cost. The shapes and corresponding parameter size lc are represented in Fig.6, where S, C and H designate the quadrangular, circular and hexagonal shapes, respectively.

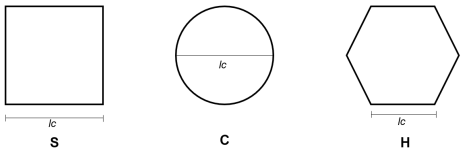

Figure 6: Crash box shapes for optimization

Nonlinear constraints were set in accordance with the Euro NCAP regulations in Tab.2,

$$\begin{cases} HIC_{15} - 700 \leq 0 \\ a_{max} - 80 \leq 0 \\ a_{3ms} - 65 \leq 0 \end{cases} . \tag{8}$$

To find the best design for the structures, 12 optimizations for each vehicle were performed corresponding to the combination of three cross shapes shown in Fig.6 and the four materials in Tab.3.

4.1 Primary front structure

The resulting Pareto sets in Fig.7 represent the junction between the simulations for each crash box with the same material for the case of the Micro Car. The same procedure was used to select the optimized structures in the other cases. The plots are organized by material: red for 6060 T64, blue for 6061 T4, green for 6061 T6 and magenta for 6082 T6; and cross shape symbols: quadrangular $\square$, circular $\bullet$ and hexagonal $\hexagon$.

Four optimal solutions were selected from the overall Pareto front, as identified in Fig.7, corresponding to the geometry and material summarized in Tab.5.

The resultant force–displacement curves during impact of the selected optimal solutions are presented in Fig.8. All curves have the same pattern and the maximum displacements

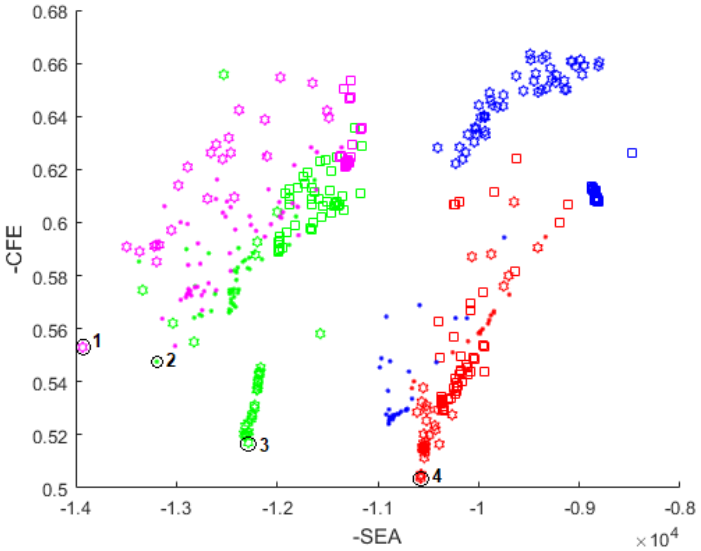

Figure 7: Final solutions for the primary front structure

Solution	CFE	SEA (J/kg)	Mass (kg)	HIC_{15}	a_{3ms} (g)	a_{max} (g)	δ (mm)	Cross shape	Material	t (mm)	lc (mm)	tl (mm)
1	0.447	13930	4.105	220.7	53.4	61.2	261.1	H	6082 T6	3.7	30.1	318.7
2	0.452	13190	4.379	233.2	57.	60.4	259.4	C	6161 T6	3.6	79.7	306.3
3	0.483	12286	4.664	232.8	55.9	56.4	248.6	H	6161 T6	4.2	29.6	318.3
4	0.496	10574	5.424	166.9	48.7	53.8	258.6	H	6060 T64	4.0	54.7	319.3

Table 5: Selected Pareto front solutions for primary front structure

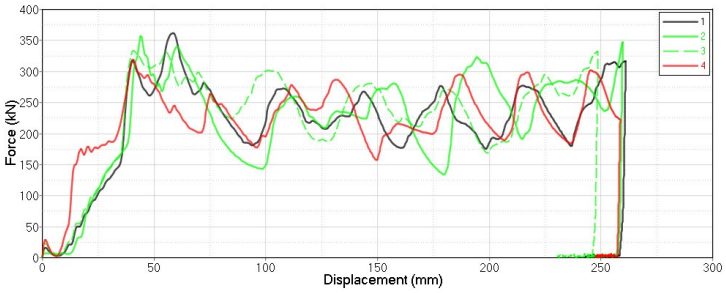

Figure 8: Force–displacement curves for selected optimal primary front structures

are almost equal. However, solution 1 has the smaller mass, result of a lower thickness, that makes it deform more easily, avoiding damage to the structures behind the bumper in case of low-speed impact. This preferred solution is represented in Fig.9.

4.2 Secondary front structure

To optimize the secondary structure, every simulation was performed including the same primary structure for every vehicle and an identical procedure to Sec.4.1 was followed.

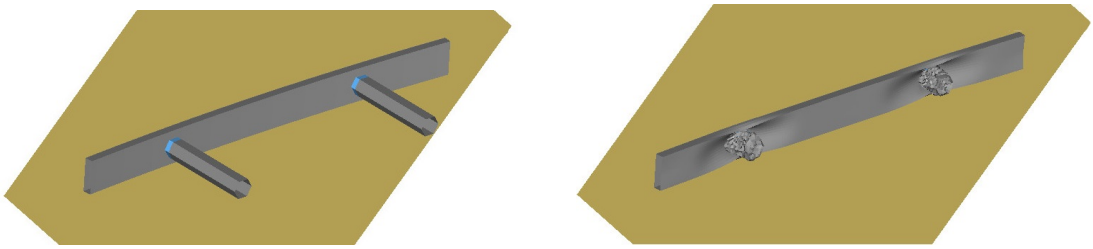

(a) before impact (b) after impact

Figure 9: Preferred optimal primary front structure in full width frontal impact

Again, the three different cross shapes given in Fig.6 and the four materials were combined and the best solutions were chosen, by analysing the values of the mass, HIC, a_{3ms}, a_{max} and δ, being their respective values summarized in Tab.6.

Vehicle	CFE	SEA (J/kg)	Mass (kg)	HIC_{15}	a_{3ms} (g)	a_{max} (g)	δ (mm)	Material	Shape	t (mm)	lc (mm)	tl (mm)	rb mm)	bh (mm)	lb (mm)
Sports Car	0.495	9945	6.728	245.7	54.0	55.2	239.3	6061 T6	H	2.0	30.1	283.4	4747	56.2	20.6
Be 2.0	0.485	10581	7.221	264.0	55.9	56.6	253.5	6082 T6	H	2.0	41.1	271.9	5608	59.5	23.0
Big Sedan	0.520	11398	7.545	188.0	48.2	52.5	247.9	6082 T6	H	2.4	43.9	304.4	4627	56.5	24.4

Table 6: Selected optimal solution for secondary front structure

4.3 Pareto Optimal Solutions

The performance of the optimally designed structures can be compared for each vehicle typology by analyzing the data summarized in Tab.7. It is possible to compare the energy

Vehicle	Primary struct.				Secondary struct.				Total					
	F_{max}	a_{max}	Mass (kg)	EA (J)	F_{max}	a_{max}	Mass (kg)	EA (J)	F_{max}	a_{max}	Mass (kg)	Δ_{mass}	EA (J)	Δ_{EA}
Micro Car	362.1	61.1	4.105	56979										
Sports Car	352.3	50.9	4.105	52113	134.4	19.4	2.623	15390	381.6	55.1	6.728		67502	
Be 2.0	348.7	44.1	4.105	54604	180.2	22.8	3.116	22463	457.0	57.8	7.221	+7.3 %	77071	+14.2 %
Big Sedan	351.6	39.5	4.105	52800	212.9	23.9	3.440	33808	555.0	62.4	7.545	+12.1 %	86607	+28.3 %

Table 7: Optimized front structures

absorption (EA) as well as the maximum peak force and the mass for each frontal crash management system. The difference columns of energy absorption and mass represented are relative to the Sports Car solution.

A better perception about the behavior of the structures is given in Fig.10 where the differences between the energy absorption and the peak force for each case are illustrated.

Analyzing Tab.7 and Fig.10, it is possible to conclude that the primary structure absorbs almost the same energy in the different crash tests. This comes from the fact that the selected optimal frontal primary geometry is not oversized for the condition

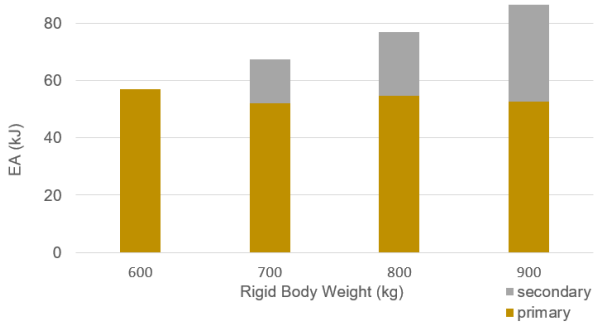

Figure 10: Energy absorption comparison for frontal crash structure

established in the 600kg test (Micro Car). Thus, the structure is totally deformed in the tests with heavier vehicles, absorbing the kinetic energy that are supposed to.

In addition, the maximum peak force is not directly related with the vehicle's mass neither with the sum of the peaks from the primary and secondary structure. This peak force is of utmost importance in the next vehicle design phase, where the structures that support the crash management systems will have to be designed to carry these loads or, in extreme cases, to deform after the entire crush of the absorbing structures to absorb additional energy.

Looking at the increase of 7.3% and 12.1% in mass of the Be 2.0 and Big Sedan relative to the Sports Car, the absorbed energy increased 14.2% and 28.3%, respectively, showing a good crash performance gain.

The final optimized front structures are shown in Figs.11, 12 and 13, where the primary structure is colored dark grey and the secondary structure in light grey.

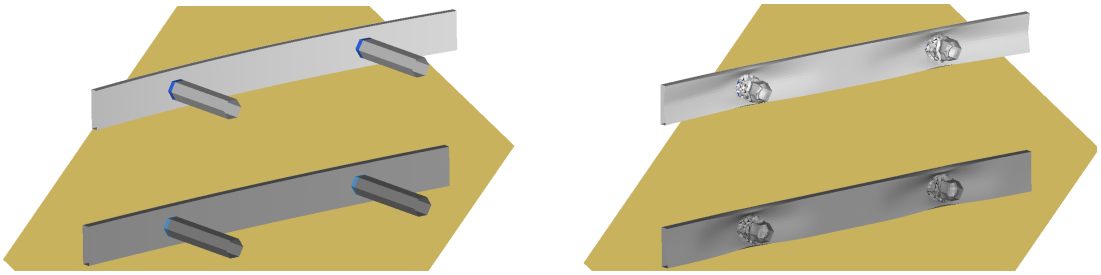

(a) before impact (b) after impact

Figure 11: Optimal Sports Car front structures in full width frontal impact

Analyzing the figures, it is noticeable the increase of robustness of the structure from the lighter to the heavier vehicle, as a result the additional kinetic energy that has to be absorbed in the impact.

The primary and secondary front structures have proven to be effective in the vehicle protection, overcoming the imposed constraints from the Euro NCAP regulations regarding full width frontal impact.

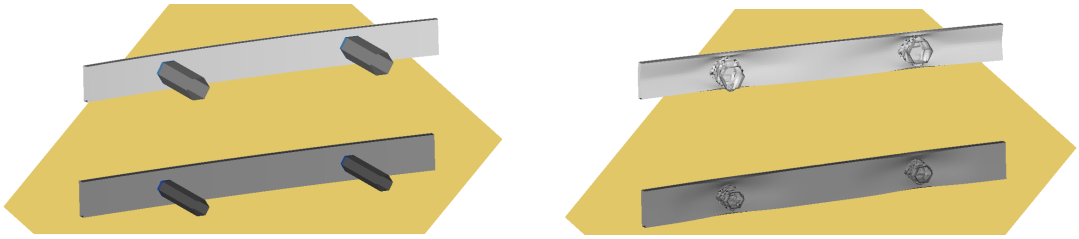

(a) before impact (b) after impact

Figure 12: Optimized Be 2.0 front structures in full width frontal impact

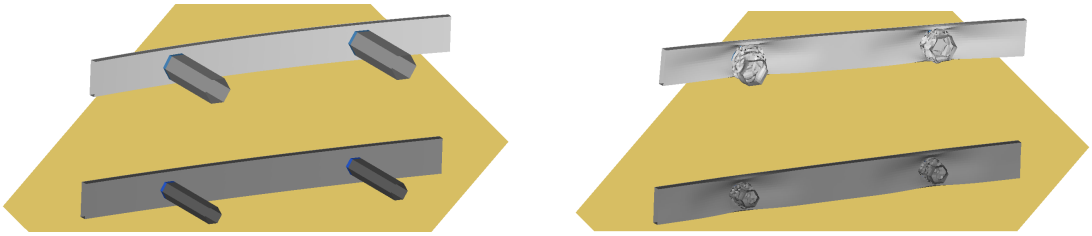

(a) before impact (b) after impact

Figure 13: Optimized Big Sedan front structures in full width frontal impact

4.4 Computational Cost Assessment

The numerical solutions required a large computational effort due to the required relatively small mesh size (8mm) and nodal time step used in the explicit time-integration scheme (0.0004ms). Table 8 shows the CPU time spent for each optimization case, where two average computer workstations were used. The required total CPU time of nearly 80 *days* was found acceptable with the usage of parallel computing.

Vehicle	Simulation time (min.)	Number of simulations	Total time (min.)
Mini Car	15	828	12420
Sports Car	27	1272	34344
Be 2.0	27	1295	34965
Big Sedan	27	1235	33345

Table 8: Simulation time for each optimization

5 OPTIMAL DESIGN OF SIDE STRUCTURE

5.1 Project Requirements

The design of the side beam for the Be2.0 chassis has to meet dimensional, structural, crashworthiness, material and fabrication requirements, applied to the project by CEiiA.

The dimensional requirements are related with the batteries and overall car size. The beam must be 140mm in height, 130mm in width, and 1660mm (supported at 1600mm) in length.

The structural requirements are related with rigidity and stress: maximum deflection of beam in vertical direction of the beam less than or equal to 1mm while bearing a load of 600kg uniformly distributed and doubly supported at its tips in static and dynamic situation; and maximum torsional deflection less or equal to 0.04rad while bearing a torque of 355.5Nm at its tip in static and dynamic situation.

The crashworthiness requirements are the most rigorous and difficult to overcome because the test applied to the beam must be as close as possible to the Euro NCAP side impact pole test. The maximum acceleration, maximum HIC_{15}, velocity and pole dimensions must be equal to this test. The structure has to withstand the impact with 800kg and must ensure that the intrusion of the beam towards the interior of vehicle be less than 150mm. To perform a more demanding test than the Euro NCAP pole test on the analyzed values, in this test, the vehicle's motion forms an angle of 90^o with the vehicle's longitudinal centerline.

Finally, the beam must be made of aluminum and manufactured by extrusion.

These requirements were either imposed in the beam definition parameters or considered as nonlinear constraints in the optimization algorithm.

5.2 Pareto Optimal Solutions

The design of the side impact thin-walled beam included three possible cross section topologies, as illustrated in Fig.14, that differed in the internal walls. Combined with

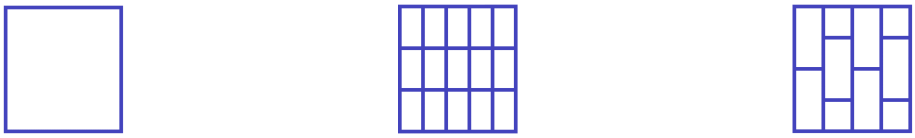

(a) rectangular (b) aligned quadrangular (c) misaligned quadrangular

Figure 14: Side beam cross-sections

different strategies in terms of internal cell widths, resulted in a total of five optimization cases: 1) rectangular shape, 2) aligned quadrangular shape, 3) misaligned quadrangular shape, 4) aligned quadrangular shape with thicker first cell walls, 5) misaligned quadrangular shape with thicker first cell walls.

In case 1, only the beam wall thickness and sectional width were optimized. As expected, the wider beam yielded greater displacement with smaller pole intrusion, so the maximum alowed beam width of 130mm was set fixed in the following cases. This case also showed that the intrusion constraint was the most critical in the optimization. As illustrated in Fig.15 in black, the CFE increase is only achieved by increasing the mass, proving the trade-off between these two objective functions. On one hand, the lightest

beam had a mass of 16.54kg but a very mediocre crash performance. On the other hand, the beam with the best crash performance had a CFE of 0.464 but with a mass increase of 57.9%. The optimal solutions obtained, though satisfying all constraints, presented a mediocre crash performance.

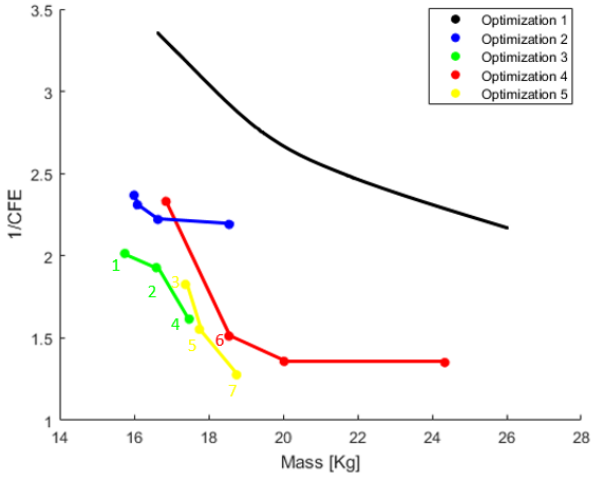

Figure 15: Pareto fronts of the five side beam topologies

From case 1 onwards, all optimizations were performed following the strategy that a larger beam deformation lead to a higher energy absorption in a lower displacement, thus with less intrusion. Also, only integer variables were allowed to optimize the number of internal cells and reduce the search area. The design variables included the number of closed cells in height nh, the number of closed cells in width nw, and the thickness $t1$ of the walls (two different parameters $t1$ and $t2$ in cases 4 and 5).

The implemented strategy was a success in case 2, the quadrangular shaped beam led to an overall increase of CFE, with the solutions from case 2 dominating those of case 1, as seen in Fig.15 in blue. However, the improvement obtained was still not sufficient since the Pareto front solutions still present a high maximum peak force: the best crash performance design had a CFE of just 0.456.

Case 3 used the strategy of having a quadrangular shape beam with the squares misaligned half their size that aimed at reducing the maximum peak force and increasing the deformation in the beam width region. The Pareto solutions are in Fig.15 in green. It yielded the lightest beam (15.75kg) that could satisfy all constraints with a CFE of 0.497, better than in any design in case 2. Also, the design with best CFE (0.619) as also obtained, for a mass of 17.48kg. Thus, compared to the lightest beam, a mass increase of 11% led to an improvement of CFE by 25%.

Cases 4 and 5 considered the thickness of the first section cell different from the rest of the cells. The rationale was to place thinner cells in contact with the pole to deform this region more easily and, consequently, reduce the initial peak force. The larger thickness

is placed in the first beam width division to increase the force after the peak, in an effort to increase the CFE. This larger thickness division acts as a barrier to intrusion and gives sufficient stiffness in the static test.

Case 4, used that multiple thickness strategy applied to the aligned quadrangular cross-section. As seen in Fig.15 in red, there was an improvement in CFE relative to the same beam without this applied strategy (case 2), ut the improvement was always followed by a mass increase. The lighter solution found in this optimization is in fact dominated by a case 2 design.

In case 5, the same multiple thickness strategy was applied to the misaligned quadrangular shape beam. The solutions shown in Fig.15 in yellow exhibit the same behavior as those in case 4, that is, The crash performance gains come at the cost of increased mass relative to case 3 designs.

Comparing the Pareto fronts of cases 2 and 3 and of cases 4 and 5, the beams with the misaligned quandrangular shape dominate almost all aligned quandrangular shape ones. In addition, comparing cases 2 and 4 and cases 3 and 5, the strategy of forcing the first beam width division to be thicker led to a substantial improvement in crash performance, despite at a cost of yielding heavier structures.

The non-dominated individuals numbered in Fig.15 from 1 to 7 constitute the global Pareto front. Their performance metrics are summarized in Tab.9. Beam designs 1 and 7

Design	CFE	Mass (kg)	HIC_{15}	a_{max} (g)	δ (mm)	Cross shape	nh	nw	$t1$ (mm)	$t2$ (mm)
1	0.497	15.75	47.00	37.21	145.71	c3	2	4	3	n/a
2	0.519	16.60	52.74	38.50	140.55	c3	4	7	2	n/a
3	0.548	17.38	50.68	37.05	148.92	c5	3	3	3	4
4	0.619	17.48	49.55	37.73	135.65	c3	2	5	3	n/a
5	0.644	17.75	37.86	28.97	142.47	c5	2	6	2	5
6	0.661	18.55	38.18	28.08	147.85	c4	3	4	2	6
7	0.784	18.75	35.14	22.63	149.58	c5	2	2	2	7

Table 9: Global Pareto front solutions for side structure

represent the lightest beam and the highest CFE, respectively, and the designs in between trade-off solutions. Although design 2 is 6.5% lighter than design 4, the later has a higher CFE of about 19%. Compared to design 3, design 4 presents a CFE about 11.5% higher for almost the same mass. The intrusion δ in design 4 is also less intrusive than those of designs 2 and 3, thus prevailing among the three. Comparing design 5 with design 6, the later presents an improvement in CFE of 2.6%, but at the cost of an additional 4.5% mass. Also, design 5 is less intrusive than design 6.

As such, designs 4 and 5 exhibit the most advantages. However, since design 5 presents an increase of about 4% in CFE with just 1.5% mass increase, together with 23% smaller maximum acceleration, it is the preferred one.

As seen in Tab.9, the preferred design is a quadrangular shape (case 5) beam with the squares misaligned and with the strategy of forcing the first width division to be thicker than the rest of the beam. It is formed by 2 cell divisions in height, 6 cell divisions in width, 2mm for thickness 1 and 5 mm for thickness 2.

In Fig.16, the curve force–displacement for the preferred side beam is represented with the maximum and average force levels highlighted. The observed proximity between the two forces levels are the result of crashworthiness optimality, that is, a reduced peak force and an extended area below the curve.

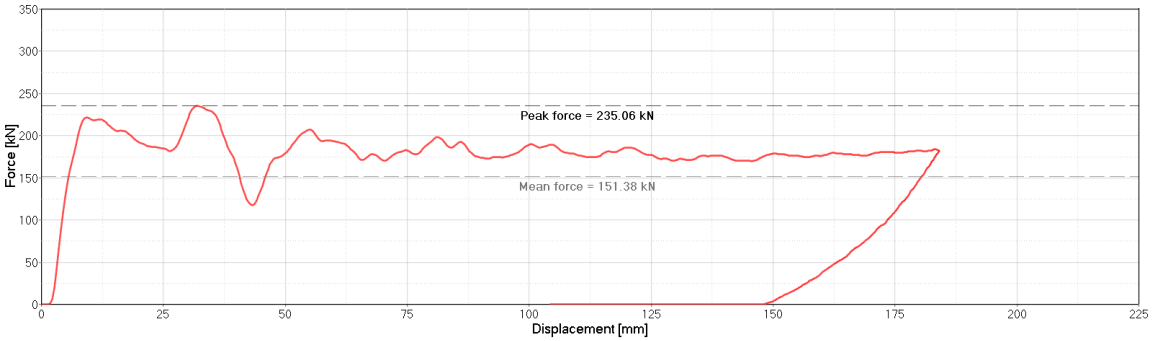

Figure 16: Force–displacement curve of the selected side beam

Figure 17 shows the result of the side impact pole test for the selected side beam, evidencing the differences between before and after crash.

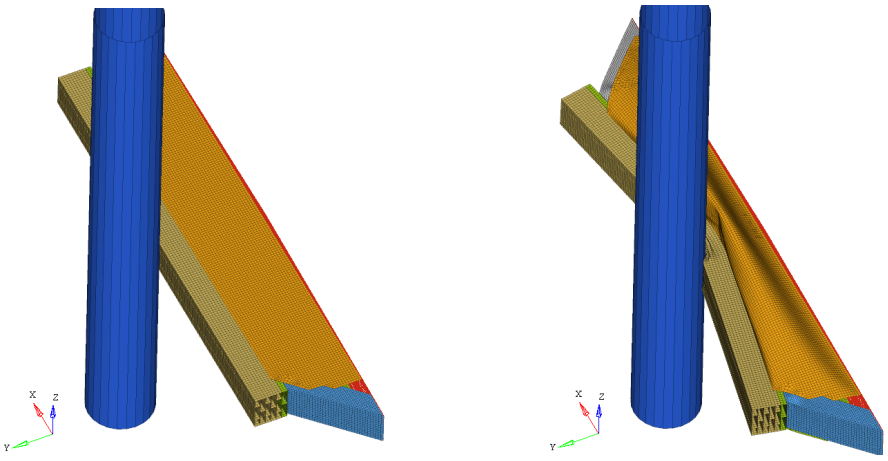

(a) Before impact (b) After impact

Figure 17: Side impact pole test simulation for the selected optimal side beam

6 CONCLUSIONS

The developed optimization process made possible to optimize different crash management systems to protect the occupants for the cases of frontal and side impacts.

The process using a *MATLAB* script to implement the multi-objective genetic algorithm *NSGA II* optimization algorithm has proven to be a great approach to obtain the desired solutions. Beside, all solutions fulfills the Euro NCAP regulations regarding the full width frontal impact and side pole impact protocols.

For the front crash structure, four different vehicle types were considered. The primary front structure revealed the desired behavior in all tests, protecting effectively the vehicle with lower mass. The optimized secondary front structure to complement the primary structure in the heavier vehicles exhibited a good trade-off between mass increase and energy absorption capability. The primary structure absorbed almost the same amount of energy in all tests, being the secondary structure responsible to absorb the additional energy from the higher vehicle mass. The Pareto front designs were mainly made with 6061 T6 and 6082 T6 alloys, since the yield strength is the most important mechanical property in crashworthiness.

As for the side beam design, also trading-off pole crash performance and structural weight, also subject to specific nonlinear constraints (HIC_{15}, acceleration, intrusion, torsional deflection, displacement in vertical direction and Von Mises equivalent stress), resulted in a set of Pareto optimal designs, from which it was possible to select the best engineering solution. Several beam cross-sections and strategies were used, but the quadrangular shape beams, with closed cells misaligned and first width division thicker than the remaining proved to be the best.

The design methodology developed can be applicable to any type of chassis, be it smaller or larger cars, mini buses or cargo vehicles, since the numerical tools are powerful and flexible enough to easily redesign crash beams for any other applications, with different geometric parameterization, objective functions and constraints.

ACKNOWLEDGEMENTS

The authors would like to thank Eng. Lus Colao for their support during this work. A word of gratitude also to CEiiA for hosting the first two authors during their internships. This work was supported by FCT (Foundation for Science and Technology) through IDMEC (Institute of Mechanical Engineering), under LAETA project UID/EMS/50022/2019.

REFERENCES

[1] European Commission Directorate General for Mobility and Transport. What are main crash injury situations? `https://ec.europa.eu/transport/road_safety/specialist/knowledge/vehicle/key_issues_for_vehicle_safety_design/what_are_main_crash_injury_problems_en`, Accessed April 2018.

[2] Anton Kuznetcov, Igor Telichev, and Christine Q Wu. Effect of Thin-walled Tube Geometry on Its Crashworthiness Performance. In *14th International LS-DYNA Users Conference*, Canada, June

2016. University of Manitoba.

[3] Xiong Zhang, Hui Zhang, and Zong Wang. Bending collapse of square tubes with variable thickness. *International Journal of Mechanical Sciences*, 106:107–116, 2015.

[4] Muhammed Emin Erdin, Cengiz Baykasoglu, and Merve Tunay Cetin. Quasi-static axial crushing behavior of thin-walled circular aluminum tubes with functionally graded thickness. *Procedia Engineering*, 149:559–565, 2016.

[5] Guangyong Sun, Fengxiang Xu, Guangyao Li, and Qing Li. Crashing analysis and multiobjective optimization for thin-walled structures with functionally graded thickness. *International Journal of Impact Engineering*, 64:62–74, 2013.

[6] Wlodzimierz Abramowicz and Norman Jones. Dynamic axial crushing of square tubes. *International Journal of Impact Engineering*, 2(2):179–208, 1984.

[7] Wlodzimierz Abramowicz and Norman Jones. Dynamic axial crushing of circular tubes. *International Journal of Impact Engineering*, 2(3):263–281, 1984.

[8] Na Qiu, Yunkai Gao, Jianguang Fang, Zhaoxuan Feng, Guangyong Sun, and Qing Li. Crashworthiness analysis and design of multi-cell hexagonal columns under multiple loading cases. *Finite Elements in Analysis and Design*, 104:89–101, 2015.

[9] N. Nasir Hussain, Srinivasa Prakash Regalla, and Yendluri V.Daseswara Rao. Comparative Study of Trigger Configuration for Enhancement of Crashworthiness of Automobile Crash Box Subjected to Axial Impact Loading. *Procedia Engineering*, 173:1390–1398, 2016.

[10] Pawe Bogusz, Micha Stankiewicz, and Grzegorz Sawiski. Energy absorption study of aluminium profiles with variety of filling configurations. *Engineering Transactions*, 65(4):543–562, 2017.

[11] Y. Chen, A. H. Clausen, O. S. Hopperstad, and M. Langseth. Stress-strain behaviour of aluminium alloys at a wide range of strain rates. *International Journal of Solids and Structures*, 46:3825–3835, 2009.

[12] S. Kokkula, O. S. Hopperstad, O. G. Lademo, T. Berstad, and M. Langseth. Offset impact behaviour of bumper beam-longitudinal systems: Numerical simulations. *International Journal of Crashworthiness*, 11(4):317–336, 2006.

[13] Kalyanmoy Deb. *Multi-Objective Optimization using Evolutionary Algorithms*. John Wiley & Sons, Ltd, 2001.

[14] European Aluminium Association. The Aluminum Automotive Manual. Applications - Car body Crash Management Systems, 2013.

[15] Jos Àngel Lpez Campos, Abraham Segade Robleda, Jos Antonio Viln Viln, Paulino Jos Garca Nieto, and Javier Blanco Cordero. Study of a steel's energy absorption system for heavy quadricycles and nonlinear explicit dynamic analysis of its behavior under impact by FEM. *Materials*, 8(10):6893–6908, 2015.